The temperature dependence of R lines in Cr^{3+}-doped forsterite

1993 J. Phys.: Condens. Matter 5 5991

(http://iopscience.iop.org/0953-8984/5/32/027)

J. Phys.: Condens. Matter 5 (1993) 5991–5996. Printed in the UK

The temperature dependence of R lines in Cr^{3+}-doped forsterite

Hiroo Komura†, Tooru Takahashi†, Isao Nasuno† and Kenji Ishikawa‡
† Department of Engineering, Shizuoka University, Hamamatsu 432, Japan
‡ Research Institute of Electronics, Shizuoka University, Hamamatsu 432, Japan

Received 26 March 1993, in final form 5 May 1993

Abstract. The fluorescence due to a purely electronic transition $^2E \rightarrow {}^4A_2$ of Cr^{3+} ions is investigated, as related to the thermal effect on peak position and linewidth in the temperature range 10–200 K. The observed characteristics of the line shift and width are analysed as the result of two-phonon Raman scattering processes, and related parameters including an effective Debye temperature are determined so as to agree with the experiments.

1. Introduction

Chromium-doped forsterite $Mg_2SiO_4:Cr^{3+}$, Cr^{4+} has attracted attention as a laser material tunable in the near-infrared region. Although a considerable number of studies [1–8] have been made on laser action and related characteristics, the fluorescence is not fully understood because of the complex fluorescence mechanism brought about by several centres differing from each other in valence and site symmetry under which they are located.

Forsterite has an orthorhombic structure belonging to a space lattice D_{2h}^{16} (or *Pbnm*) and four formula units of Mg_2SiO_4 in its unit cell. The impurity ion Cr^{3+} or Cr^{4+} occupies an Mg^{2+} or an Si^{4+} site respectively and each behaves as a fluorescent centre. It has been found that the Cr^{4+} ion in a tetrahedral site is associated with laser action in the wide region of wavelength centred at 1235 nm, while the Cr^{3+} ion with $3d^3$ electronic configuration is responsible for red and near-infrared emissions (680–950 nm) accompanied by fine structures [6].

The situation in forsterite is different from that in ruby $Al_2O_3:Cr^{3+}$, where trivalent chromium ions are located in a slightly distorted O_h (or $m3m$) crystal field. In forsterite they substitute Mg ions of two kinds whose symmetries are classified as C_i (or $\bar{1}$) and C_s (or m). These sites are often called M1 (inversion) and M2 (mirror) as for alexandrite $BeAl_2O_4:Cr^{3+}$ in the same situation. In this paper, however, we designate the inversion and mirror sites as Cr^{3+}(I) and Cr^{3+}(II) after Weiyi Jia *et al* [6] to avoid confusion because M1 and M2 are sometimes used to denote pure electronic transitions of magnetic-dipole origin. For the fluorescence observed in the red and near-infrared region, the existence of two centres with different site symmetry in forsterite, and phonon participation in the transitions, generates a complex fine structure, which can be resolved into pure electronic transitions and their phonon sidebands. The relevant pure electronic transitions due to the Cr^{3+} ion are from excited states $^2E(Cr^{3+}(I))$, $^2E(Cr^{3+}(II))$ and $^4T_2$ to a common ground state $^4A_2$ in successive order of photon energy of the emission. The purpose of this report is to discuss the temperature dependence of the well known purely electronic transitions, R lines ($^2E \rightarrow {}^4A_2$), in forsterite. Accordingly, the more intense fluorescence, originating from Cr^{3+}(II) and Cr^{4+} ions, located in the longer-wavelength region, is out of our scope.

0953-8984/93/325991+06$07.50

2. Experimental details

The specimen used in the present experiments was a synthetic single-crystal cube of side 5 mm, which was grown by the Czochralski method by Mitsui Mining and Smelting Co. This biaxial crystal cube was so cut as to have each crystal axis perpendicular to a cube face. The chromium concentration was found to be around 0.17 at.%.

Emission spectra were measured at various temperatures down to 10 K using an Oxford CF-100 helium flow-type cryostat. Fluorescence was excited by the 488 nm line of an Ar ion laser GLG-3300 (NEC) at a power level up to 200 mW, and led to a Jobin–Yvon HG-2S Ramanor double monochromator. In the 680 nm region, the instrument offers an overall resolution of 0.5 cm^{-1}, sufficiently sensitive for measuring the linewidth. Detection was carried out with a conventional photomultiplier and photon counting equipment HTV-C767 (Hamamatsu Photonics) with a microcomputer control system. The signal-to-noise ratio was improved by averaging repeated scannings. When the polarization characteristics of the fluorescence were to be measured, a quartz wedge was placed in front of the entrance slit of the monochromator to exclude the polarization characteristics of the detection system by spatially scrambling the polarized light incident on the monochromator.

3. Temperature dependence of R lines

In figure 1 the red fluorescence is shown for a particular optical configuration. Sharp R lines and their phonon sidebands are clearly observed. We now concentrate our attention on the R lines originating from a transition $^2E(Cr^{3+}(I)) \rightarrow {}^4A_2$. This purely electronic transition is further split into R_1 ($\bar{E}$: 693 nm, 14430 cm^{-1}) and R_2 ($2\bar{A}$: 683 nm, 14641 cm^{-1}) lines by the low field symmetry in forsterite. The correspondence of $\bar{E}$ and $2\bar{A}$ to R_1 and R_2 depends on the sign of two trigonal-field parameters. It has been proved that R_1 is associated with $\bar{E}$ and R_2 with $2\bar{A}$ in ruby and *vice versa* in Cr^{3+}-doped spinels [9, 10]. Hence, the assignment for forsterite is rather tentative because the polarity of the trigonal field has not yet been established.

Purely electronic transitions associated with R lines are forbidden as electric-dipole transitions for the Cr^{3+} emission centres with high symmetry. They appear in general as weak emissions of magnetic-dipole origin, but as relatively intense emissions of electric-dipole origin when the crystal-field symmetry is reduced by lattice distortion. In uniaxial crystals, comparison of the π-, σ- and α-polarization patterns is used to determine whether the pure electronic transition is electric or magnetic in dipole character. Thus, it has been found that R lines are of magnetic-dipole character in MgO:Cr^{3+} and of electric-dipole character in ruby [11]. In the present experiment for biaxial forsterite, all the possible configurations were investigated to determine the dipole character of the R lines. If the intensity does not change much, for example, between two different configurations for the electric vector of emitted light with the magnetic vector fixed to a crystal axis, but changes among different configurations for the magnetic vector of the emission, then the purely electronic transition would be assigned as one associated with the magnetic dipole. Figure 2 shows how the integrated intensity of the R_1 line depends on the polarization characteristics of the emission. No relationship can be recognized among the integrated intensities of the R_1 lines for different optical configurations. The situation is the same for the R_2 lines. In addition, the integrated intensity ratio of the associated phonon sidebands to the R lines is found to be in the range 3–5. This is too low for the case where the R lines are regarded as pure magnetic-dipole transitions. Usually, the ratio is much larger for

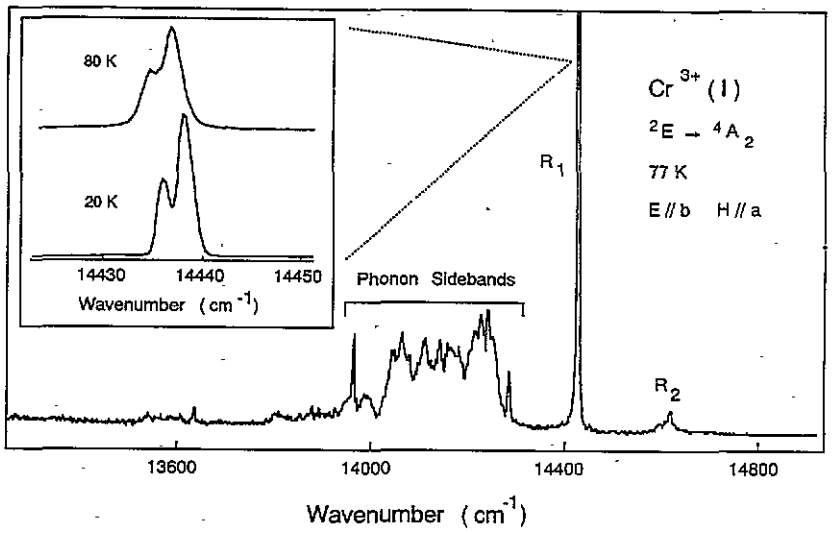

Figure 1. Red emission spectra from Cr^{3+} ions with inversion symmetry. The emission was excited by the 488 nm line (200 mW) of an Ar ion laser. An optical configuration between electric (magnetic) vector $\boldsymbol{E}$ ($\boldsymbol{H}$) of fluorescent light and crystal axes is assigned as $\boldsymbol{E}\|b$, $\boldsymbol{H}\|a$ in this figure. R_1 and R_2 lines are generated from a pure electronic transition ^2E ($2\bar{A}$ and $\bar{E}$)$\rightarrow$ $^4A_2$ and corresponding phonon sidebands are observed on the lower-energy side of these lines. The doublet structure of the R_1 line, shown in the inset, is due to splitting of the ground state and is observed at a temperature lower than 80 K. The spectrum at 80 K is shifted upward for convenience but the relative intensity and peak positions between the two spectra (80 K and 20 K) are conserved.

the set of a purely electronic transition of magnetic-dipole character and its sideband of electric-dipole character, e.g. 65 for the R_1 line and its sideband for the Mn^{4+} ion with the same $3d^3$ electronic configuration as the Cr^{3+} ion [12]. Therefore, the R lines in forsterite are essentially of magnetic-dipole character but are partially of electric-dipole character since the lower-symmetry field in forsterite may loosen the selection rule for electric-dipole transitions. More informative experimental techniques are required for the rigid assignment of dipole character in R_1 and R_2 lines [13].

The integrated-intensity ratio between two R lines was measured at various temperatures and the temperature dependence was found to be ruled by the Boltzmann law. A temperature dependence of the ratio should be expected since thermal excitation changes the population ratio between the split states $2\bar{A}$ and $\bar{E}$. The splitting in ruby is too small (29 cm^{-1}) to cause strong temperature dependence since the two states are almost equally populated at high temperatures, whereas in forsterite it is large enough (211 cm^{-1}) for a dependence to be observed in the temperature region of the present experiments.

As a result, the R_2 line would disappear at sufficiently low temperature, and actually faded out below 50 K in our case. The observed ratio is described in terms of η exp $(-\Delta E/kT)$, where $\Delta E(= 211\ cm^{-1})$ is an energy separation between R_1 and R_2. The proportional constant η was found to be 3.7 for configurations $\boldsymbol{E}\|b$, $\boldsymbol{H}\|a$ and larger than unity for all possible configurations. Values larger than unity indicate that a difference between the selection rules exists for the downward transitions from the two excited states $\bar{E}$ and $2\bar{A}$ to the ground state $^4A_2$. The transition rate is lower for R_1 ($\bar{E}$) than for R_2 ($2\bar{A}$).

Figure 3(*a*) and (*b*) shows the temperature dependence of peak position and full width at half maximum (FWHM) for R_1 and R_2 lines respectively for a configuration $\boldsymbol{E}\|b$, $\boldsymbol{H}\|a$.

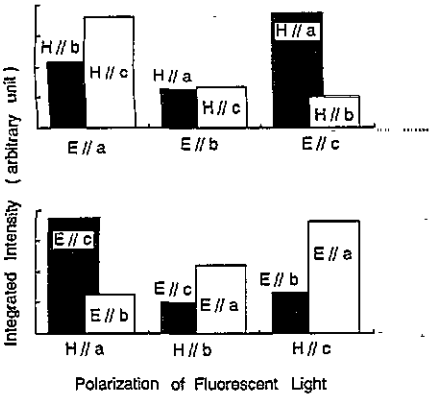

Figure 2. Integrated intensity of the R_1 line for all possible optical configurations. The difference due to the direction of the magnetic vector of light relative to the crystal axes when the electric vectors are fixed should be noted in the upper part of the figure, and *vice versa* in the lower. No relationship is recognized among the configurations. This indicates that the R lines originate from both magnetic and electric dipoles.

Similar characteristics are also observed for other configurations. The enlarged line profile of the R_1 line is found in the area shown in the inset of figure 1, where the R_1 line separated from the R_2 line by a low crystal field is observed by itself as a doublet. Splitting of the doublet (2.3 cm^{-1}) is caused by the spin–orbit interaction in the ground state $^4A_2$ [6]. Two isolated peaks, clearly observed at liquid helium temperature, are obscured with increased temperature. The superposed doublet must be separated into individual peaks to determine the peak position and FWHM for each peak. The observed R_1 line is reproduced as the superposition of two components, each of which is calculated individually as the hybridization of weighted Gaussian and Lorentzian shape functions. The best fit is obtained at each temperature by assuming an appropriate hybridization ratio. At 20 K, for example, the line shape is formed from 95% Gaussian and 5% Lorentzian shape functions. Only the peak positions are shown in figure 3(*b*) for R_2 because the R_2 line is not detected clearly enough that the FWHM can be determined by resolving the doublet.

There is a review article by Powell and DiBartolo [14] reporting optical properties of ruby, where the dependence of peak position and FWHM on temperature is discussed in detail [14, 15]. The peak position of a purely electronic transition is described as

$$\nu = \nu_0 - \alpha(T/T_D)^4 \int_0^{T_D/T} x^3(\exp x - 1)^{-1}\,dx$$

where ν_0, α and T_D are respectively the peak position with no phonon participation, a coupling parameter and an effective Debye temperature. This expression is obtained when the two-phonon Raman scattering process is the main contribution to peak shift, and direct phonon processes (absorption and emission) are negligible. Among these parameters, ν_0 can be determined to be 14 436 cm^{-1} as the centre of gravity obtained from two R_1 components observed at the lowest temperature. The observed data of temperature dependence can be best fitted when $\alpha = 345$ cm^{-1} and $T_D = 490$ K (340 cm^{-1}). The experiment at high temperatures is well reproduced. As for the observed peak positions below 80 K, the position of the centre of gravity for two components should be compared with the calculation. Since two individual peaks are illustrated in figure 3(*a*), it must be mentioned that calculation agrees excellently with the observed values when compared with their centres of gravity.

For the R_2 line, another set of parameters must be assumed: $\alpha = 220$ cm^{-1} and $T_D = 440$ K (305 cm^{-1}) ('calculated 1' in figure 3(*b*)) since those parameters used for R_1 do not give the best fit to the observed data ('calculated 2' in figure 3(*b*)). In this procedure, ν_0 is assumed to be 14 633 cm^{-1}, the R_2 peak position observed at the lowest temperature.

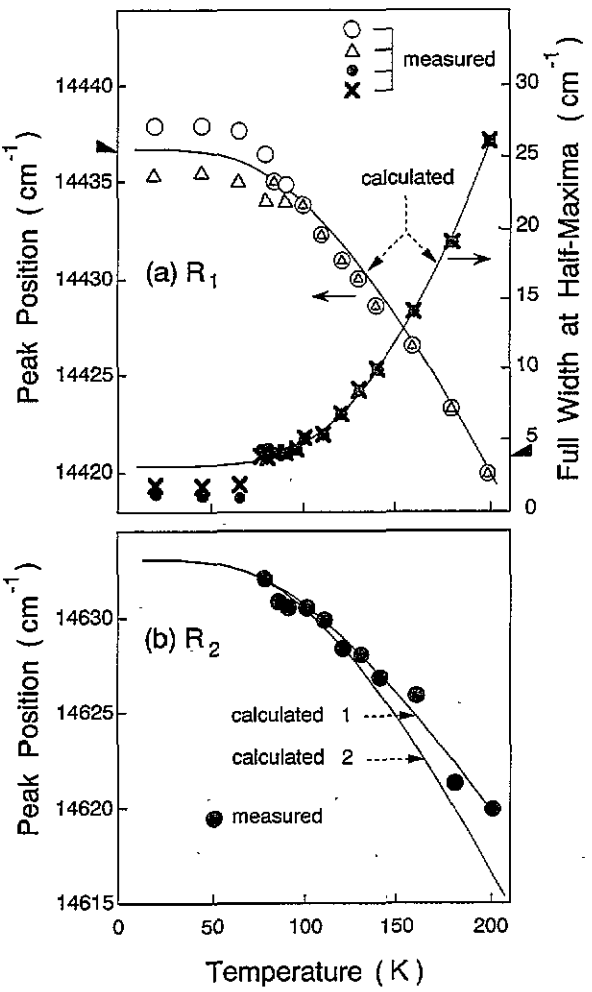

Figure 3. Temperature dependence of peak position and full width at half maximum for (*a*) R_1 and (*b*) R_2. At low temperatures, the R_1 line is observed as two isolated peaks. Calculations must be compared with the centre of gravity on peak positions (the averaged wavenumber of two individual peak positions when the intensity ratio is considered as a weighting coefficient) and with the sum of linewidths of each component. The locations obtained experimentally at the lowest temperature are indicated by a wedge on the left or right ordinate respectively.

It is natural that when the temperature is increased, the R_1 line due to purely electronic transitions has a much broader linewidth than one brought about by inhomogeneous broadening. The actual FWHM is broadened by the electron–phonon interaction added to the linewidth already determined by inhomogeneous (strain) broadening, owing to the fluctuation of local crystal field around each fluorescent centre. At comparatively higher temperatures, two-phonon Raman scattering processes cause line broadening with a Lorentzian shape function superposed on the Gaussian function due to strain broadening [16]. It is known that direct phonon absorption and emission processes make a small contribution to the FWHM as well as to the temperature dependence of peak position [14, 15]. The expression describing the FWHM is written as follows:

$$\Delta\nu = \Delta\nu_0 + \bar{\alpha}(T/T_D)^7 \int_0^{T_D/T} x^6 \exp x (\exp x - 1)^{-2}\, dx$$

where $\Delta\nu_0$, $\bar{\alpha}$ and T_D correspond respectively to the original linewidth due to strain broadening, a coupling parameter and an effective Debye temperature. Our result shown in figure 3(*a*) is well described when $\Delta\nu_0 = 3.5$ cm^{-1}, $\bar{\alpha} = 2000$ cm^{-1} and $T_D = 640$ K (445 cm^{-1}) are assumed. The linewidth must be discussed for the total width of R_1 above 80 K, although the linewidth of each component can be determined below that temperature. The sum of the individual linewidths of R_1 components is taken as a virtual linewidth $\Delta\nu_0$ for strain broadening, although individual linewidths below 80 K are shown in figure 3(*b*).

4. Conclusion

The R lines associated with purely electronic transitions in forsterite show typical aspects of their thermal shift and line broadening when the temperature is increased. These can be attributed to two-phonon Raman scattering processes. Empirical data can be well described by assuming appropriate parameters in a theoretical framework.

References

[1] Petricevic V, Gayen S K, Alfano R R, Yamagishi Y, Anzai H and Yamaguchi Y 1988 *Appl. Phys. Lett.* **52** 1040–2
[2] Petricevic V, Gayen S K and Alfano R R 1988 *Appl. Phys. Lett.* **53** 2590–2
[3] Verdun H R, Thomas L M, Andrauskas D M, McCollum T and Pinto A 1988 *Appl. Phys. Lett.* **53** 2593–5
[4] Petricevic V, Gayen S K and Alfano R R 1989 *Opt. Lett.* **14** 612–4
[5] Moncorge R, Cormier G, Simkin D J and Capobianco J A 1991 *IEEE J. Quantum Electron.* **QE-27** 114–20
[6] Weiyi Jia, Huimin Liu, Yen W M and Denker B 1991 *Phys. Rev.* B **43** 5234–42
[7] Sugimoto A, Segawa Y, Nobe Y, Yamagishi Y and Yamaguchi Y 1991 *Japan. J. Appl. Phys.* **30** L495–6
[8] Glynn T J, Imbush G F and Walker J 1991 *J. Lumin.* **48 & 49** 541–4
[9] McClure D S 1962 *J. Chem. Phys.* **38** 2757–79
[10] Wood D L, Imbush G F, Macfarlane R M, Kisliuk P and Lakin D M 1968 *J. Chem. Phys.* **48** 5255–63
[11] Henderson B and Imbusch G F 1989 *Optical Spectroscopy of Inorganic Solids* (Oxford: Clarendon) pp 284–5
[12] Donegan J F, Glynn T J, Imbush G F and Remeika J P 1986 *J. Lumin.* **36** 93–100
[13] Yamaga M, Henderson B, Marshall A, O'Donnell K P and Cockayne B 1989 *J. Lumin.* **43** 139–46
[14] Powell R C and DiBartolo B 1972 *Phys. Status Solidi* a **10** 315–57
[15] DiBartolo B 1968 *Optical Interactions in Solids* (New York: Wiley) pp 371, 374
[16] McCumber D E and Sturge M D 1963 *J. Appl. Phys.* **34** 1682–984